Heliyon 10 (2024) e32281

Contents lists available at ScienceDirect

Heliyon

journal homepage: www.cell.com/heliyon

Research article

Fabrication of alcohol sensor using undoped and Al doped ZnO nanostructure film with polymer electrolyte gating

Raju Bhattarai [1], Ram Bahadur Thapa [1], Deependra Das Mulmi [2], Rishi Ram Ghimire [1,*]

[1] Patan Multiple Campus, Department of Physics, Patandhoka, Lalitpur, Nepal
[2] Nepal Academy of Science and Technology, Khumaltar, Lalitpur

ARTICLE INFO

Keywords:
EDL gate dielectric
Field effect transistor sensor
Al doped ZnO
Polymer electrolyte

ABSTRACT

We report the fabrication of two terminal and three terminal gas sensor using Al-doped ZnO nanostructured-films and polymer electrolyte gate dielectric on glass substrate using vacuum free chemical method. The Al doped ZnO films are characterized by UV–vis Spectrometer, SEM, EDX and XRD. The characterization results have revealed the polycrystalline structure of both undoped and doped ZnO; with loosely packed, porous, and spherical granny nanostructure with mean grain size 20–10 nm and bandgap of the films is within the range of 3.12–3.16 eV. The conductivity of the ZnO film is tuned by Al concentration and the maximum value of conductivity was observed in 3 % Al doped ZnO films. Similarly, the best performance index of TFT such as current ON/OFF ratio, high transconductance and low threshold voltage was observed in 3 % Al doping concentration. The ordinary (two-terminal) sensor and three-terminal (FET) sensors' responses towards three different concentrations 50, 250, 500 ppm of ethanol and methanol vapors have been studied. The sensitivity of the film is modulated by Al concentration and higher value of sensitivity was achieved at 3 % Al doped ZnO films. The use of polymer electrolyte enhanced the sensitivity of the device which is more effective in methanol vapor. The Response-Recovery time of the sensor is significantly improved in three terminal devices than the two terminal devices.

1. Introduction

Gas sensing technologies have attracted much more attention of the scientific community, industry, and academia with increasing applications of industrial productions, medicines, automotive, indoor air quality control, environmental monitoring, etc. Due to the versatile applicability and intrinsic drawbacks of various gases, different scenarios with enhanced gas sensor calibration are being explored by researchers [1]. Semiconducting metal oxides like ZnO, Fe_2O_3, SnO_2, TiO_2, CuO, and WO_3 are strong and well-researched material for gas sensing applications. Several oxide-based nanostructures such as nanoparticles, thin films, nanorods [2], and nanowires have been synthesized and employed to fabricate gas sensors. It's obvious that chemical components of sensing materials, surface states, microstructure and morphology play significant role in gas sensing performance. Among the various oxide semiconductors, ZnO, a wurtzite structured wide direct-band gap (around 3.2eV) semiconductor, is promising candidate due to its strong shape, size, and surface tenability. It is non-toxic, eco-friendly, cost-effective and easy to synthesize [2,3]. The surface of ZnO is depleted due to the

* Corresponding author.
E-mail address: rishighimire34@gmail.com (R. Ram Ghimire).

https://doi.org/10.1016/j.heliyon.2024.e32281
Received 14 September 2023; Received in revised form 30 May 2024; Accepted 31 May 2024
Available online 7 June 2024

absorption of gases from the environment. Thus, the electrical conductivity of ZnO can be drastically changed in exposure to reactive/toxic gases existing in the environment [4]. Introducing foreign elements like Al, Cu, Ag, etc.in appropriate amount in ZnO modifies its surface morphologies and shape leading to increased conductivity and sensitivity. The defect states of ZnO may change with doping concentration, which has a higher role in carrier transport phenomena. Also, doping Aluminum makes the film more transparent and has huge application in fabrication of optical detector [5].

The moderately high carrier mobility, surface and shape tenability, easy functionalization and doping are the major strength of ZnO. Despite its numerous advantages, nanostructured ZnO faces challenges such as slow response, sample inhomogeneity, and lack of reproducibility, especially in chemically grown films [6]. These drawbacks can be mitigated through doping, functionalization, and surface treatment, which enhance the performance index in electronic and optoelectronic applications.

In this study, an alternative method is proposed to control ZnO channel resistance using polymer electrolyte, facilitating surface modification without altering its stoichiometry. The electrostatic effect of polymer electrolyte on the ZnO surface can be controlled by applying bias voltage in a three-terminal device [6]. The study aims to compare two-terminal and three-terminal ZnO-based gas sensors using polymer electrolyte to enhance sensitivity and response time.

Conventional oxide-based gate dielectrics in field effect devices have been superseded by polymeric electrolyte gate dielectrics because of its high carrier accumulation strength especially in oxide material and relevancy in field effect transistor (FET) with nanostructured channel where regulating grain boundary (two crystallites-interface) charges substantially controls charge transport in the channel. The electric double layer (EDL) formed by polymer electrolyte with ZnO surface induces huge surface charges which enhance the mobility and the drain current (current through the semiconductor channel) by passivizing the charge defects and changing the occupancy of defect states [7]. Filed effect transistor configuration is a popular electrochemical sensor used as a transducer for over 40 years. In many reports conventional oxide materials are used as gate dielectric which requires high vacuum technology. Here we have used the polymer electrolyte in gel form and drop cast on ZnO surface which is simple cost-effective vacuum free method and have high performance index even used for flexible electronic [8]. Although several reports have discussed gas sensors using ZnO material, none have explored gas sensors using polymer electrolyte as a gate dielectric. This study aims to address this gap by investigating the behavior of ZnO-based sensors with gated polymer electrolyte.

In this work the transducer has two major components one is ZnO channel which generate the electrical signal after imposing

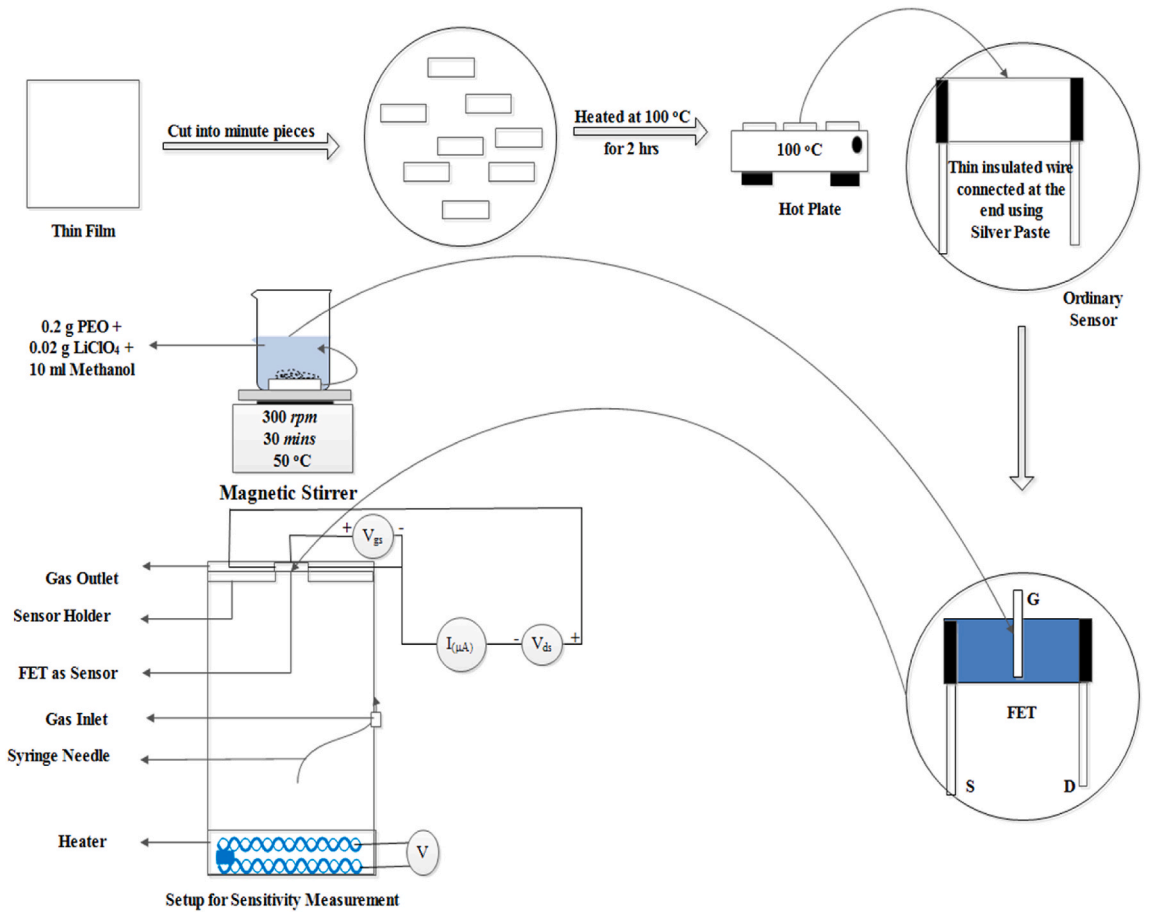

Fig. 1. Fabrication of FET as a sensor and setup for sensitivity measurement [12].

analyte gas and another is the polymer electrolyte which is also sensitive to the analyte. The polymer electrolyte surface directly interacts with target analyte and the ZnO channel converts this interaction to electrical signal. Whenever the target analyte (gas) interacts with polymeric dielectric, it proliferate electrons as freebie to the EDL dielectric polymer which leads to an immense enhancement in drain current. As soon as the gas is removed, atmospheric oxygen molecules are further adsorbed and supplied Gate-Source voltage begins to stabilize the charge in the EDL minifying the drain current back to its former value [9]. The control of the sensor is directly linked with applied gate bias [10].

The research involves doping various concentrations of aluminum on nanostructured zincoxide films and evaluating their conductivity. The 3 % concentration of aluminum-doped ZnO film shows promising results for fabricating thin-film transistors (TFTs) using $LiClO_4$ and Polyethylene Oxide (PEO) as gate dielectric. Interestingly, the use of polymer electrolyte dielectric in the two-terminal device fabricated with 3 % aluminum-doped ZnO film enhances sensitivity to methanol vapor, achieving fast response and recovery times in three-terminal devices.

Overall, the primary objective is to compare the performance of two-terminal and three-terminal ZnO-based gas sensors using polymer electrolyte. The aim of the study is to explore how gas sensors can achieve a remarkable boost in sensitivity and quick response by employing polymer electrolytes and create high-quality FET for gas sensing applications, particularly for monitoring alcohol vapor.

2. Methodology

The approaches that had been taken for the entire fabrication of sensor and its application process are summed up in following steps.

2.1. Deposition of thin film

Among various methods for deposition of thin film like electro-chemical deposition method, chemical vapor deposition (CVD), pyrolysis, molecular-beam epitaxy (MBE) [11] and so on, spin coating was found budget and lab-frame feasible because of its plainness, cost-efficacy, simplistic doping approach, ordinary operating temperature, and regulative spin and film width [12]. The substrate is rotated at high speed after drop-casting a very few amounts of coating material over it to distribute the material uniformly all over it then annealed to evaporate excessive solvent. The procedure can be repeated until reaching the desired thickness or film-resistance [8–11].

For 0.5 M pristine ZnO precursor solution, Diethyl Amine (DEA-6 ml) and Zinc Acetate Dihydrate (ZAD-13.3872 g) added to Ethanol (120 ml) was whirled (300 rpm) for about an hour at normal temperature [12]. For 0.5 M dopant solution, 1.91 g Aluminium Nitrate added to Ethanol (20 ml) was stirred under same circumstances. Under similar conditions, varying dopant (Aluminium Nitrate Solution) volume (0.2, 0.4, 0.6, 0.8, and 1.0) in ml were added to precursor (Zinc Acetate) of volume (19.8, 19.6, 19.4, 19.2, and 19.0) in ml for doping 1 %, - 5 % of Aluminium respectively and stirred as illustrated in Fig. 1.

Additionally, precursor solution (0.1 ml) was cascaded over spinning substrate (3000 rpm) held in a spin-coater, allowed to spin for 30 s to achieve uniformly distributed film and then annealed at 550 °C for a quarter-hour [12].

2.2. Fabrication of sensor

After films fabrication, they were cut into small fragments of around 3 × 7 mm and warmed up for 2 hours at 100 °C. During heating process, thin wires were joined to the extremities of the films with silver paste which eventually works as ordinary sensors. A cylinder of around 300 cm^3 volume is fitted with two heaters: top one for film temperature regulation and bottom one to volatilize alcohol (if necessary). The syringe needle is adjusted as presented in Fig. 1 to enable gas passage or liquid droplets onto the heater [12]. This is the way, how ordinary sensors were constructed using fabricated thin films.

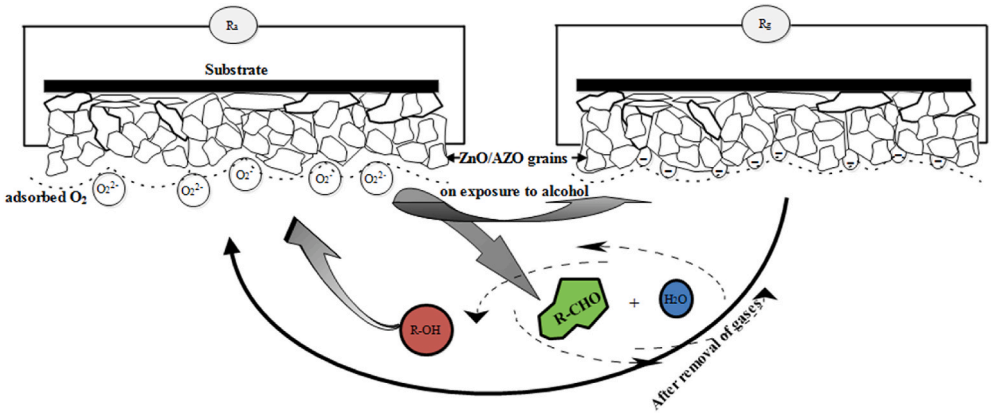

Fig. 2. Sensing Mechanism of ZnO/AZO thin Film.

The EDL gate electrolyte was prepared by stirring 0.2 g of Polyethylene Oxide (PEO) and 0.02 g of Lithiumchlorate ($LiClO_4$) in 10 ml of Methanol at 300 rpm, and 50 °C for 30 min. The same procedure of constructing an ordinary sensor was followed; then, the contacts between the wire and film were insulated using glue and a single drop of electrolyte was drop cast and spread over the channel. Subsequently, an insulated thin wire, conducting at the ends, was gently placed over the electrolyte, and the device was allowed to dry. Once the electrolyte dried, for device stability, source and drain wires across the channel and gate wire over the electrolyte were fixed onto a Printed Circuit Board (PCB) by soldering, and the substrate was glued. These were the procedures followed to construct the Thin Film Transistor (TFT). The device was then ready for further characterization and application. As illustrated in Fig. 1, for sensitivity measurement by FET, the ordinary sensor at the top of the former setup was replaced by the fabricated FET.

2.3. Sensing Mechanism

The exposed surface of ZnO film loses its free electrons to oxygen molecules forming charged layer of molecular/dissociative type adsorbate (O_2, O_2^-/O_2^{2-}) in its grain boundaries leading high resistance and potential barrier, as presented in Fig. 2. The ethanol/methanol vapor when exposed gets oxidized to CO_2, CO, and H_2O potentially undergoing dehydrogenation or dehydration. However, since ZnO is n-type oxide, dehydrogenation is preferred [12,13]. Eventually, when the electrons are released back, the conductivity of the film increases and resistance deducts [10,12]. The film's response to alcohol vapors depends on formation of aldehydes from alcohol as follows:

$$2C_2H_5OH \rightarrow 2CH_3CHO + H_2 \quad (1)$$

$$2CH_3CHO\ (ad) + 5O_2^{2-}(ad) \rightarrow 4CO_2 + 4H_2O + 10e^- \quad (2)$$

$$2C_2H_5OH\ (ad) + O_2^{2-}(ad) \rightarrow 2C_2H_4O^-(ad) + 2H_2O \quad (3)$$

$$2C_2H_4O^-(ad) \rightarrow CH_3CHO\ (ad) + e^- \quad (4)$$

$$CH_3OH\ (g) \rightarrow CH_3OH\ (ad) \rightarrow CH_3O(ad) + H\ (ad)\ [[13]] \quad (5)$$

When the vapor is no longer present, the film begins re-adsorption of oxygen and tends to achieve its initial state [10], as represented in Fig. 3. Electric double-layer (EDL) gated thin-film transistor has emerged as a roseate candidate, garnering considerable attention due to its substantial ion-induced capacitance at semiconductor/electrolyte interface, sensitive interfacial features, low voltage operation and potent gating effect strong enough to modulate the carrier density of the semiconductor channel with remarkable efficacy.

The conversion of alcohol vapors into aldehydes due to adsorption of Oxygen at the grain boundary region [11,13] is analogous to bare films. However, in this context, the adsorption effect influences the interfacial potential and enhances the channel current through an EDL capacitive coupling effect [9].

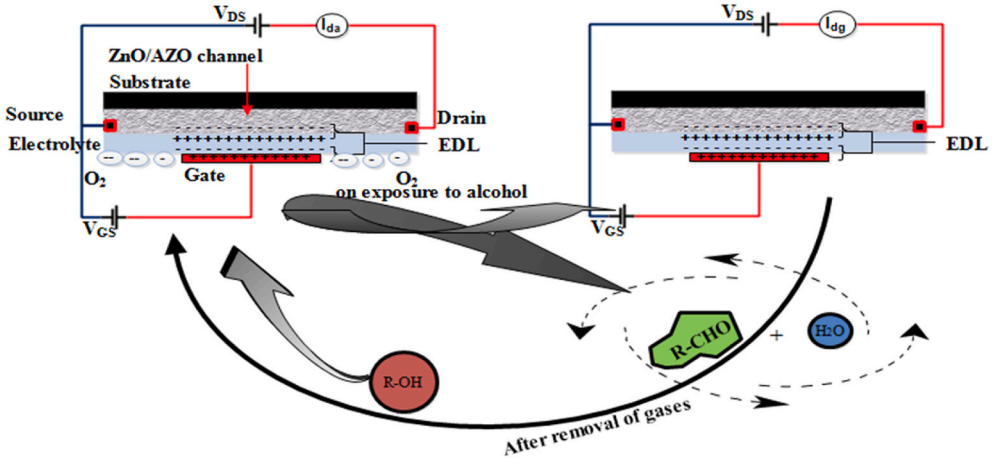

Fig. 3. Sensing Mechanism of EDL gated TFT.

3. Results and discussion

3.1. UV–vis Spectroscopy

The measurements of absorbance/transmittance of film samples were taken for further analysis and calculation of film-bandgap using "UV–Vis spectrophotometer (Carry 60 spectrophotometer, Agilent Technology)" at "Nepal Academy of Science and Technology (NAST)". For direct transition, the absorption coefficient varies with photon energy and optical bandgap of nanostructure film can be determined using Tauc's-plot method,

$$(\alpha h\nu)^{0.5} = A\left(h\nu - E_g\right) \quad \text{(Eq. 1)}$$

Where, 'α' represents absorption coefficient, 'A' represents a constant, 'E_g' denotes optical bandgap and 'h' denotes plank constant. When $(\alpha h\nu)^{0.5}$ is extrapolated to 0, it gives energy band gap of the films [14].

The Tauc's Plot of Pristine ZnO and various concentrations of A:ZnO thin films are plotted as shown in Fig. 4(a–f) and bandgaps were evaluated accordingly.

It's evident that as Al-dopant increases, Al-ions tend to replace Zn from ZnO planes and eventually the direct bandgap of the films increases. This phenomenon elongates transport path of charge carriers within the lattice and results in a significant decrease in grain size. Additionally, upon Al doping in ZnO, electrons accumulated at the lower edge of conduction band jump to excited states within the conduction band, necessitating additional energy. This process effectively broadens the optical bandgap of the film [5].

Here, the bandgap of pristine ZnO is measured at 3.120 eV, while 1 % Al-doped ZnO thin film exihibits a bandgap of 3.124 eV. As dopant concentration increases, the optical bandgaps gradually increase, reaching 3.155 eV.

3.2. X-ray diffraction (XRD)

The structural analysis of fabricated thin-films was done using XRD (Bruker D2 Phaser/1.54184 Å CuKα radiation) at operating voltage 40 KV and 40 mA current at NAST. The Debye Scherrer's relation calculates average size of grain 'D', which is given by,

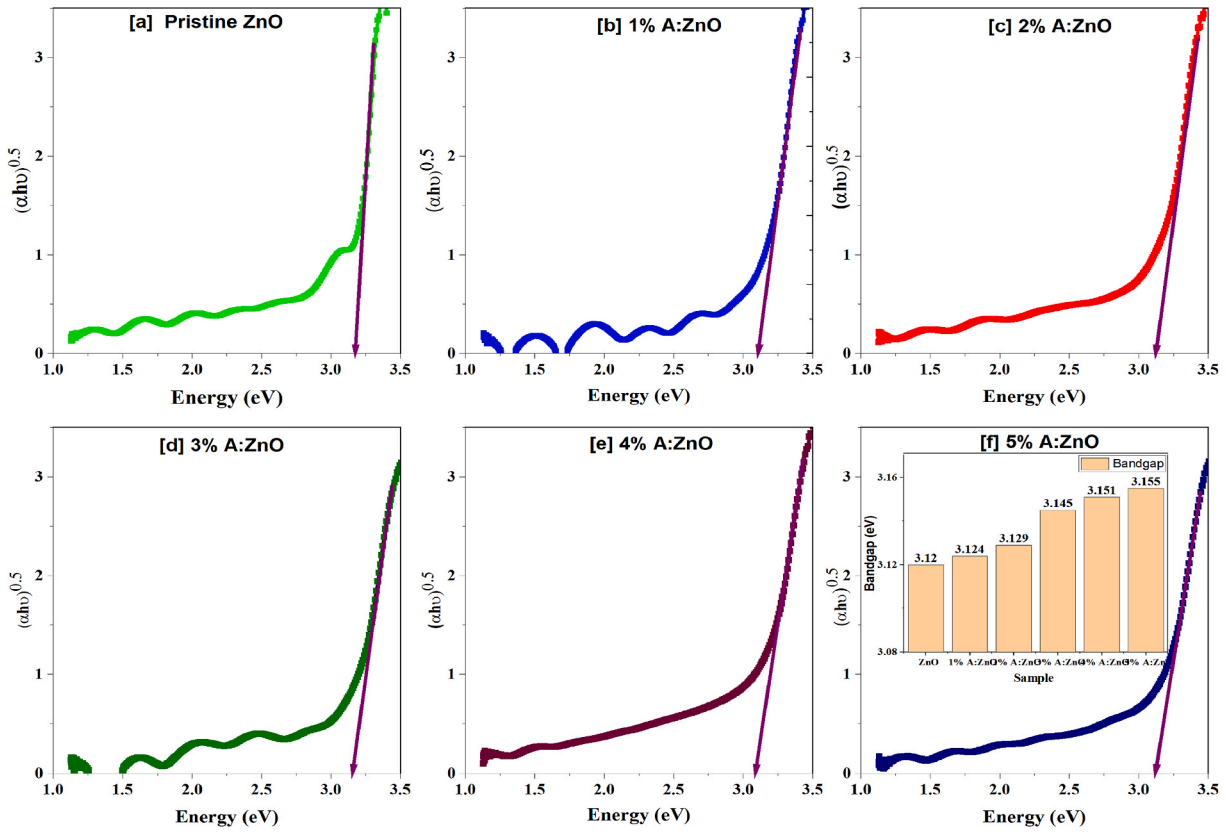

Fig. 4. Calculation and Comparison of Bandgap Energy of pristine [a] ZnO thin film and [b-f] various concentrations of Al-doped ZnO films using Absorbance.

$$D = \frac{0.9\lambda}{\beta \cos\theta} \quad \text{(Eq. 2)}$$

where, "0.9 is correction factor, λ denotes wavelength of x-ray, β denotes FWHM (full width at half maximum) of the peak observed and θ represents Bragg's angle". The d-spacings calculated are compared with the JCPDS standard-values (36–1451 card number), and indexing of the peaks are done.

Figs. 5 and 6, significantly shows that all the peaks are seen around 33.01°, 35.61°, 37.43°, 48.70°, 57.70°, 63.92°, and 69.01°, corresponding to (100), (002), (101), (102), (110), (103) and (112) respectively. These observations indicate that the films possess a hexagonal crystallite structure or are polycrystalline in nature. In addition, no significant shifts in XRD peaks are observed in Al-doped ZnO films compared to ZnO films, except for the peaks of (100), (002), and (101). Increasing doping concentration alters the peaks intensity and width, and minor peaks such as (102), (110), (103), (200) appear to diminish, while the three major peaks (100), (002) and (101) notably decrease due to Al-incorporation in ZnO lattice [5]. The shifts of (100), (002), and (101) peaks of AZO films towards larger angles, as observed in Figs. 5 and 6, is attributed to the substitution of Zn- ions by Al-ions into film's hexagonal lattice. Additionally, shifts in ZnO films are due to presence of Aluminium as impurity from its glass substrate [15].

Also, the average grain size can be calculated using Williamson Hall method, whose equation is given by,

$$\beta \cos\theta = \frac{k\lambda}{D} + \gamma \sin\theta \quad \text{(Eq. 3)}$$

Where, "k denotes shape-factor, λ denotes incident wavelength, β is the FWHM; measured in radians, D denotes average grain-size, γ denotes lattice strain and θ denotes Bragg's angle at diffraction peak".

The lattice spacing parameter 'd' was calculated using relation:

$$d = \frac{\lambda}{2 \sin\theta} \quad \text{(Eq. 4)}$$

Further, for the hexagonal crystal structure, the lattice spacing 'd' can be calculated using the relation:

$$\frac{1}{d^2} = \frac{4\left(h^2 + hk + k^2\right)}{3a^2} + \frac{l^2}{c^2} \quad \text{(Eq. 5)}$$

Where, "'h', 'k', and 'l' are miller indices, and 'a', and 'c' are lattice constants".

The particle size was determined using Sherrer's equation (Eq. (2)) and was found to be around 20 nm, 16 nm, 15 nm, 13 nm, 12 nm and 11 nm respectively. This significant decrease in particle size upon doping and increasing doping concentration is attributed to the incorporation of Aluminium atoms in place of Zinc atoms within the lattice site [5].

3.3. Scanning Electron Microscope (SEM) and EDX analysis

The EDX analysis and SEM images attached herewith was carried out using "Scanning Electron Microscope at Research Center for Eco-Environmental Science, Chinese Academy Science, Beijing, China". These SEM images shown in Fig. 7 depict loosely packed, porous, spherical and homogeneously arranged granny nanostructure. The porosity and surface roughness seem to be decreased on doping Al and again, increase in the dopant concentration has increased the roughness of the films too. The morphology of the sensing films has significant role in gas detection. Thus, porous surface with small grain size is considered to possess better gas sensitivity [16]. The uniformity of the film seems poor and may not be suitable for optoelectronic devices [17] but it has less impact in gas detection,

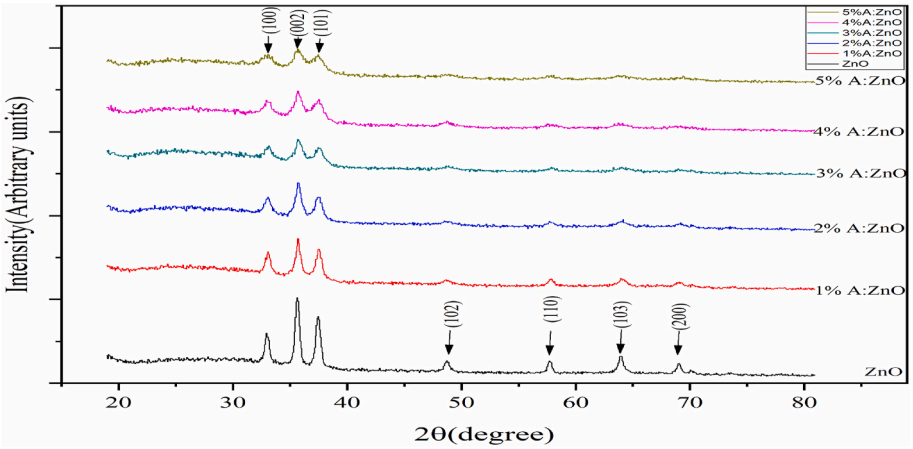

Fig. 5. XRD pattern of undoped and A:ZnO thin films labelled in legends.

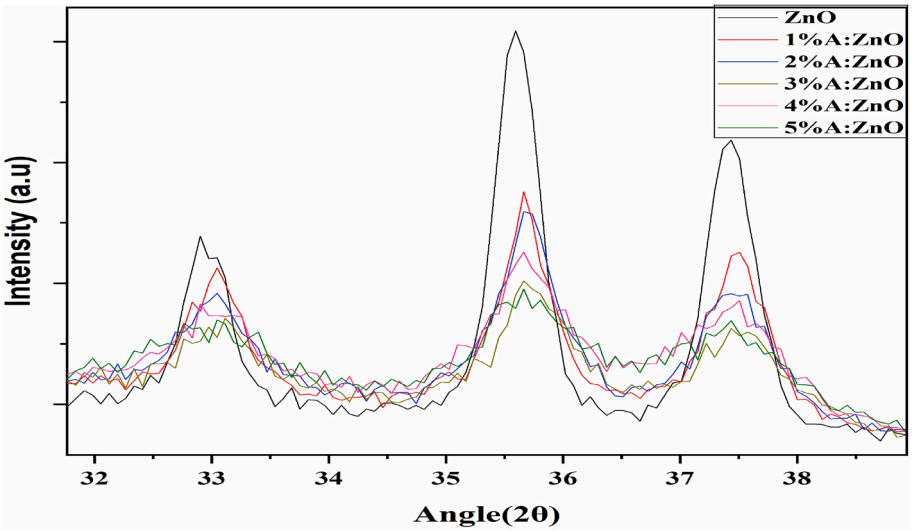

Fig. 6. XRD Pattern of ZnO and AZO corresponding to (100), (002) and (101).

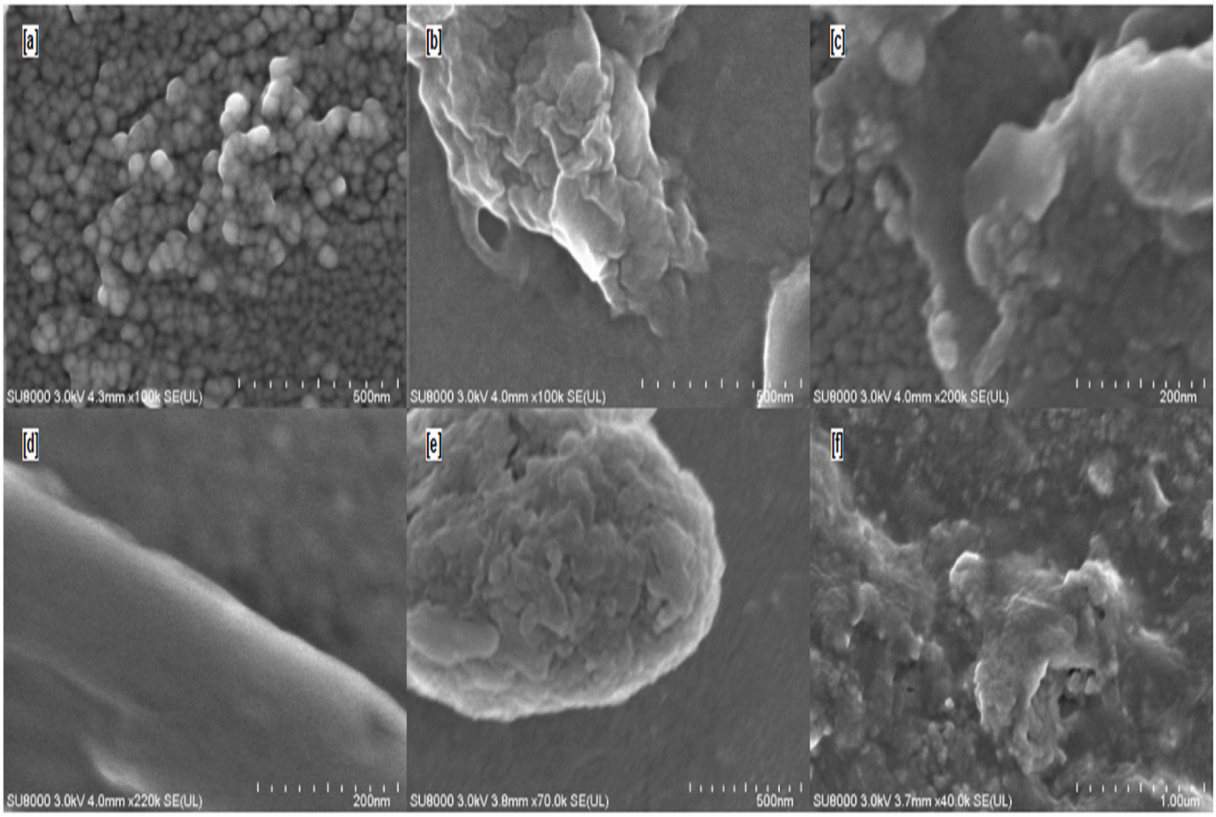

Fig. 7. SEM Images of [a] Pristine ZnO thin film [12] and [b-f] 1 %–5 % Al-doped ZnO thin films respectively.

thus can be used as gas sensor.

The EDX analysis of small region of samples was carried out as indicated in Fig. 8(c–h) and the data presented in Fig. 8(a and b) confirms that the film composition is of elements zinc and oxygen in pristine ZnO film and Zinc, Oxygen and Aluminum in AZO films without any other impurities. Aluminium Silicate in composition of glass substrate is responsible for negligible wt. % of Al found in the film of pristine ZnO [12]. Increasing doping concentration has increased wt. %, but it does not resemble doping by volume concentration anymore which may be due to inhomogeneity in distribution of Al in the precursor during its preparation. Also, it may be due to

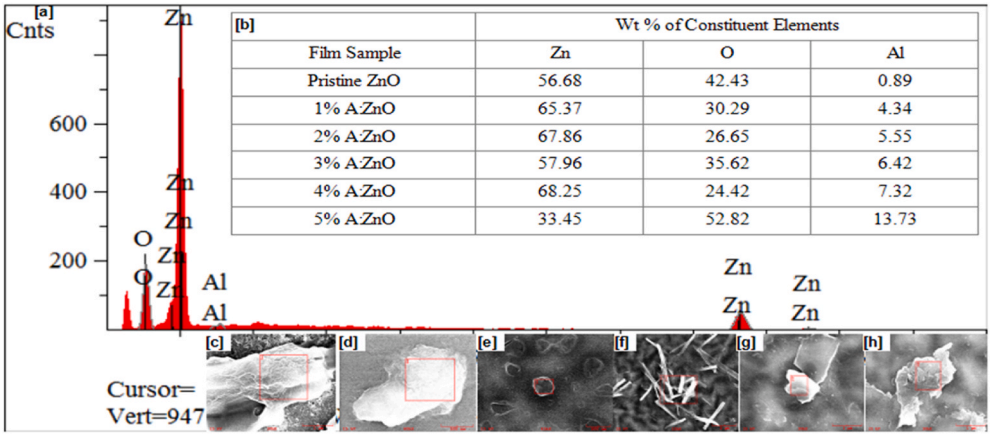

[b]

Film Sample	Wt % of Constituent Elements		
	Zn	O	Al
Pristine ZnO	56.68	42.43	0.89
1% A:ZnO	65.37	30.29	4.34
2% A:ZnO	67.86	26.65	5.55
3% A:ZnO	57.96	35.62	6.42
4% A:ZnO	68.25	24.42	7.32
5% A:ZnO	33.45	52.82	13.73

Fig. 8. [a] EDX analysis image of 3 % A:ZnO, [b] table representing wt. % of constituent elements in undoped and different concentration of Al-doped thin films, [c-h] SEM images of selected area of ZnO and different concentrations of A:ZnO thin films over which EDX analysis was done.

the fact that EDX analysis is done by selecting a very little area of about 100 nm^2 which is one out of 400 billion parts of the film prepared. So, the data of wt. % of Zinc and Oxygen seem quite erratic. Though the data, in overall, convince the film is homogeneous.

3.4. Resistivity of thin films

The electrical resistivity of ZnO and AZO is calculated using four probe technique using the relation

$$\rho = \frac{2\pi s V_{ds}}{I} \quad \text{(Eq. 6)}$$

Here, two outer probes are supplied with constant current (I) and inner probe-potential (V_{ds}) developed is measured, given that the distance (s) between all the four probes is equal [18]. The value of resistivity of the film is found decreasing when the temperature of the specimen is raised. This is due to the fact that when temperature of the specimen rises, the thermally-excited electrons move towards the conduction band increasing carrier mobility. The resistivity of ZnO and AZO films calculated from eq (6) at various temperatures is graphed in Fig. 9.

The value of resistivity is found minimum for 3 % Al-doped ZnO film at all temperatures and is found maximum for pristine ZnO sample at all temperatures. However, on increasing Al-concentration above 3 % by volume, the film resistivity increases significantly. When a trivial quantity of Al is pioneered as dopant, Ionized Al (Al^{3+}) displaces Zn^{2+} yielding a free charge (e^-) responsible for the increment of carrier concentration. Therefore, carrier concentration increases or resistivity decreases with increasing Al doping for first 3 % by volume [19]. On further increment of dopant-concentration, increasing Al dopant atom may form neutral defects and may not donate free electron and eventually electrically active dopant atoms may reduce [2,19,20]. This is the reason for the further decrement of the carrier concentration and resistivity increment.

3.5. Field effect transistor (FET) characteristics

The principal of transfer characteristics is the most important factor in evaluation of performance of TFTs which has been presented

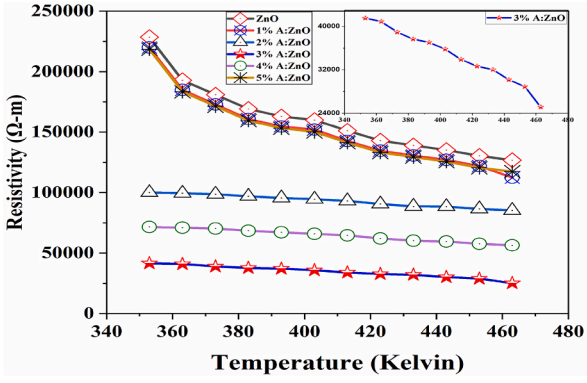

Fig. 9. Resistivity of pristine ZnO and various concentration of Al doped ZnO varying with temperature.

in Fig. 10 below. The transfer characteristics of undoped and A:ZnO films are studied keeping drain-source voltage (V_{DS}) equals 1 V and varying gate-source voltage (V_{GS}) from negative of 3 V to positive 4 V and the corresponding changes in drain current (I_d) are noted. I_d versus V_{GS} graph termed as "Transfer characteristics" is plotted and respective ON-OFF ratios i.e. ratio of maximum stable drain current to minimum stable drain current are calculated. The minimum stable current i.e. drain current of OFF-state of EDL gated 3 % Al-doped ZnO TFT is found 6 x 10^{-4} μA and maximum stable current i.e. drain current of ON-state is found approximately 115 μA. The transfer characteristic of 3 % Al-doped ZnO is found fantabulous as expected as its ON-OFF ratio is found to be maximum (~40800) among the rest of the films which may endow the higher sensitivity. So, its drain characteristics were further studied keeping V_{GS} constant (−1 V–4 V) and vary ing drain-source voltage from 0 V to 5 V and noting the corresponding changes in drain current.

The drain characteristic of the concerned sample is too found conspicuous which is as shown in Fig. 11 below.

3.6. Sensitivity of the sensors

The attenuation of film-resistance is prominent in two-terminal sensors and variation of channel current is kenspeckle in three-terminal sensors, so the sensitivity of the two-terminal sensor is calculated using the relation:

$$s = \frac{R_a - R_g}{R_a} \times 100\% \quad \text{(Eq. 7)}$$

Where, 's' stands for sensitivity, R_a and R_g are resistances of the two-terminal sensors before and after exposure to alcohol vapors [9].

For the three-terminal sensor, slight modification i.e. resistances are expressed in terms of current in relation (7) is done and calculated as:

$$s = \frac{I_g - I_a}{I_g} \times 100\% \quad \text{(Eq. 8)}$$

where 's' stands for sensitivity, I_a and I_g are channel current of the EDL electrolytic polymer gated TFT sensors before and after exposure to alcohol vapors. Here, R_a is replaced by I_g so as to obtain the sensitivity within the range of 0–100 %. Else, sensitivity more than 150 % would have been obtained which seems quite impractical.

Sensing within room temperature had been a challenge that we have successfully tackled. Three different concentrations (50 ppm, 250 ppm, 500 ppm) of alcohol vapors were passed into the setup shown in Fig. 1, and the response/recovery times, and corresponding decrease in the values of resistances were noted. The sensitivity of the two-terminal sensors i.e. bare films and EDL coated films at room temperature are calculated using relations 7 and 8, tabulated as in Table 1 and their corresponding graphs are shown in Fig. 12(a and b); Fig. 12(a) and b representing % sensitivities of the samples in response to ethanol and methanol respectively.

The higher sensitivity of the films to higher concentrations of alcohol vapors can be attributed to the increased number of alcohol molecules present. With more molecules available, there is a greater likelihood of interaction with the film's grain boundary, leading to a more significant reduction in resistance. The sensitivity of bare films to ethanol is consistently greater than that to methanol. This difference arises from the lower oxidation potential of ethanol (−0.66 V) compared to methanol (−0.55 V). Substances with higher electro-oxidation potentials, like methanol, are more resistant to oxidation, resulting in lower sensitivity [21]. Notably, the 3 % Al-doped ZnO consequently demonstrated higher sensitivity across all the tested concentration of both methanol and ethanol. This could be attributed to its smaller resistivity, smaller grain size, and rougher surface, all factors favoring sensitivity enhancement.

The application of an EDL electrolyte coating over both bare pristine ZnO and various concentrations of Al-doped ZnO sensors significantly enhance sensitivity, albeit with some variability. Interestingly, the electrolyte demonstrates a remarkable response to

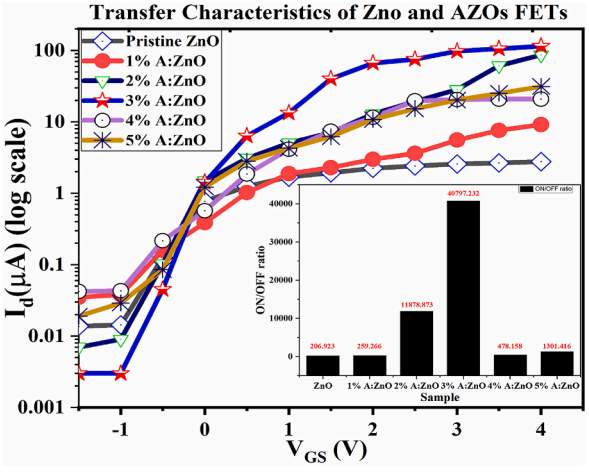

Fig. 10. Transfer Characteristics of ZnO and AZOs channeled, EDL gated TFTs.

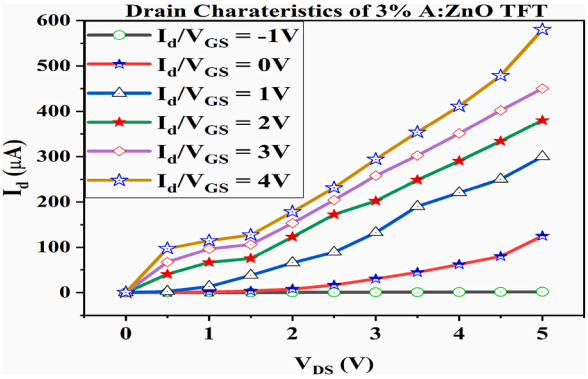

Fig. 11. Drain Characteristics of 3 % Al-doped ZnO channeled, EDL gated TFT at various Gate-Source Voltages.

Table 1
shows Sensitivity of Bare and EDL coated thin film sensors in response to varied concentrations of Methanol and Ethanol Vapors.

Gas Concentration	Sample	Sensitivity of Bare Films in response to		Sensitivity of EDL coated Films in response to	
		Methanol	Ethanol	Methanol	Ethanol
50 ppm	**ZnO**	0.86	2.41	26.05	2.61
	1%AZO	1.02	2.44	28.97	5.41
	2%AZO	1.13	2.86	30.16	11.97
	3%AZO	0.63	2.91	30.33	13.68
	4%AZO	0.43	1.82	24.38	6.73
	5%AZO	0.33	1.50	21.46	5.71
250 ppm	**ZnO**	34.25	38.41	65.19	41.72
	1%AZO	36.79	40.91	68.18	43.69
	2%AZO	41.69	47.89	79.47	48.89
	3%AZO	44.22	49.24	80.06	49.75
	4%AZO	36.05	37.92	65.02	38.69
	5%AZO	33.70	34.60	61.06	36.59
500 ppm	**ZnO**	75.85	82.56	90.51	83.95
	1%AZO	77.39	85.00	92.80	92.27
	2%AZO	85.38	93.00	96.80	97.80
	3%AZO	85.76	96.07	97.08	97.81
	4%AZO	79.33	80.57	89.04	69.12
	5%AZO	71.36	73.13	87.40	63.20

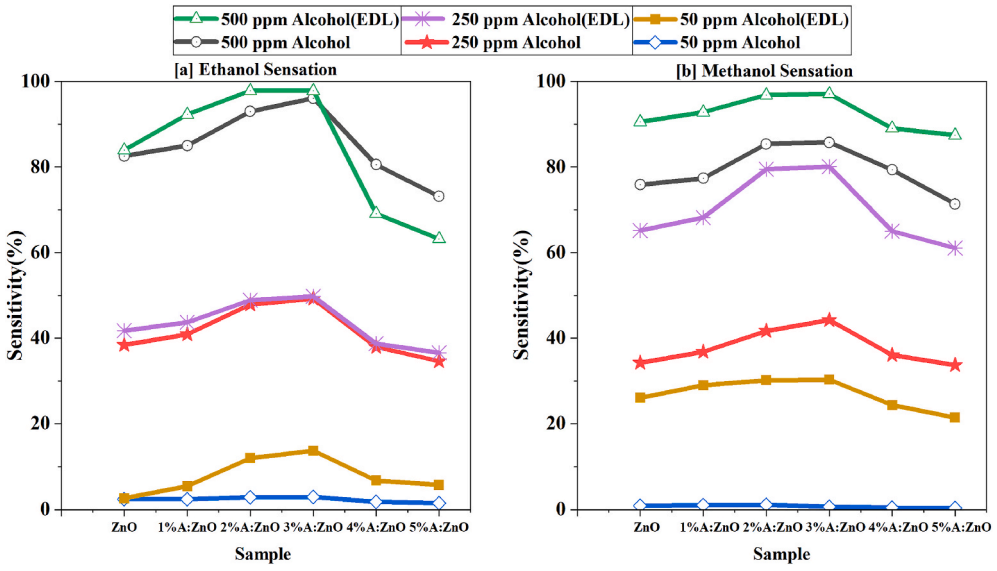

Fig. 12. Sensitivity of Bare and EDL layered Two-Terminal Sensors in response to [a] Ethanol and [b] Methanol Vapors.

methanol compared to ethanol vapors, possibly due to its composition, which might be biased towards methanol due to its use in the preparation of the electrolyte polymer.

3.7. Response and recovery of two terminal sensors

The time it takes for the film to reach its minimum resistance upon exposure to a reducing gas is termed the response time, while the time it takes for the film to recover almost 90 % of its initial resistance after the gas is removed is termed the recovery time. Experimental investigations were conducted to determine the response and recovery times of fabricated sensors. Changes in resistance of both bare and EDL dielectric polymer-coated ZnO and AZO films in response to alcohol (ethanol and methanol) vapors were monitored over time, diagrammed as in Fig. 13, and analyzed to calculate response/recovery times.

Consistently, the response time of the sensor was found to be shorter than the recovery time. Given the excellent performance of AZO film with 3 % Al-dopant compared to others. Its response to 500 ppm of alcohol vapors was specifically graphed and presented in Fig. 13.

For 500 ppm vapors, the response time for bare and EDL dielectric polymer coated 3 % Al-doped ZnO sample is found to be 13 s and 12 s in response to ethanol vapors, 15 s and 15 s in response to methanol vapors and the recovery time for the concerned sample is found to be 75 s and 60 s in response to ethanol vapors and 95 s and 75 s in response to methanol vapors respectively.

Consistently, the response/recovery times for ethanol vapors are observed to be shorter than those for methanol vapors, which could be attributed to the lower oxidation potential of ethanol.

3.8. Sensitivity of three terminal sensors

Varied concentrations of alcohol vapors were introduced into the setup depicted in Fig. 1 while maintaining the FETs in the ON state. The response and recovery times, along with the corresponding increase in drain current values, were recorded. The sensitivity of the three-terminal sensors, i.e. FETs, is computed using equation (8), and their respective graphs are displayed in Fig. 14(d); the corresponding drain current in the sample transistors before and after exposure of gas are graphed in Fig. 14(a–c).

The variations in sensitivity of thin-film FET sensors fabricated from ZnO and different compositions of Al-doped ZnO and featuring EDL dielectric polymer gating to varying concentrations of methanol and ethanol were examined. Sensitivity levels ranged from 5.65 % to 70.11 % across different compositions and analyte concentrations. In response to 50 ppm of methanol, sensitivities range from 5.65 % to 12.75 %, while for 50 ppm of ethanol, they range from 7.36 % to 16.79 %. The sensitivity levels increase with higher concentrations of analytes, reaching ranges of 18.98 %–49.70 % for 250 ppm of methanol and 24.35 %–53.82 % for 250 ppm of ethanol. At even higher concentrations, such as 500 ppm of methanol and ethanol, sensitivities escalate further, reaching ranges of 41.49 %–66.81 % and 53.91 %–70.11 %, respectively. Specifically, 3 % Al-doped ZnO consistently exhibited higher sensitivity compared to other compositions. Notably, the sensitivity of 4 % Al-doped ZnO neared that of 3 % Al-doped ZnO.

The higher sensitivity to ethanol compared to methanol, even at equal concentrations, can be ascribed to the lower oxidation potential of ethanol vapor. Additionally, the sensitivity of TFTs sensors to higher concentrations of alcohol vapors is notably higher. This increase in sensitivity can be attributed to the larger number of alcohol molecules present in higher concentrations, leading to a greater reduction in oxygen molecules from the grain boundary of the polymer. This reduction results in a significant enhancement in the channel current of the film.

Furthermore, the 3 % Al-doped ZnO channeled EDL electrolyte polymer gated TFT sensor demonstrates higher sensitivity due to its low resistivity value and sufficiently large ON-OFF ratio of around 40800 ($>10^3$). These characteristics contribute to its heightened sensitivity in detecting alcohol vapors.

3.9. Response and recovery of three terminal sensors

The time it takes for the film to reach its maximum drain current upon exposure to a reducing gas (alcohol vapors) is termed the response time, while the time it takes to return its initial drain current value (with a +5 % tolerance for convenience) after the gas is removed is termed the recovery time. Experimental trials were conducted to determine the response and recovery times of sensors. The notable changes in channel current of the EDL dielectric polymer-gated, ZnO, and AZOs channeled thin-films in response to ethanol and methanol vapors over time were recorded, plotted, and used to calculate time of response and recovery. Consistently, the sensor's time of response was found to be shorter than the recovery time. Given the excellent performance of the Al(3 %):ZnO sample compared to other samples, its response to both 500 ppm of ethanol and methanol vapor was specifically graphed, as depicted in Fig. 15.

In response to 500 ppm, for the 3 % Al-doped ZnO channeled EDL gated TFT sample, the time of response and recovery-time were found out to be 5 s and 25 s respectively, in response to ethanol vapors, and 8 s and 27 s, respectively, in response to methanol vapors. It's noteworthy that the response time for ethanol vapors was consistently shorter than that for methanol vapors, which may be attributed to the lower oxidation potential of ethanol. Moreover, it's evident that the response time is consistently shorter than the recovery time.

The production of water vapor during the oxidation of alcohol vapors when they interact with the EDL polymer may take a few more seconds to evaporate. This phenomenon could account for the observed outcomes.

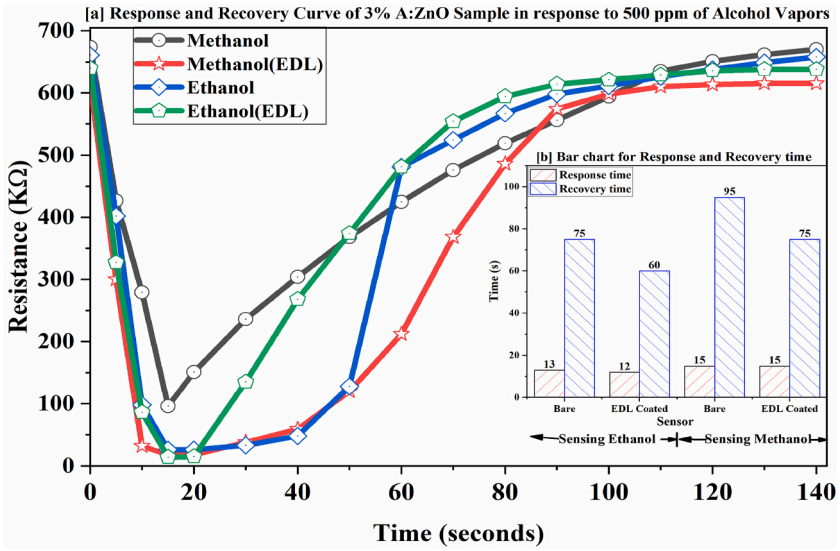

Fig. 13. [a] Variation in Resistances of Bare and EDL Layered 3 % A:ZnO films with respect to time in response to Ethanol and Methanol Vapors [b] Bar chart for response and recovery time of Bare and EDL coated 3 % A:ZnO thin-film sensors.

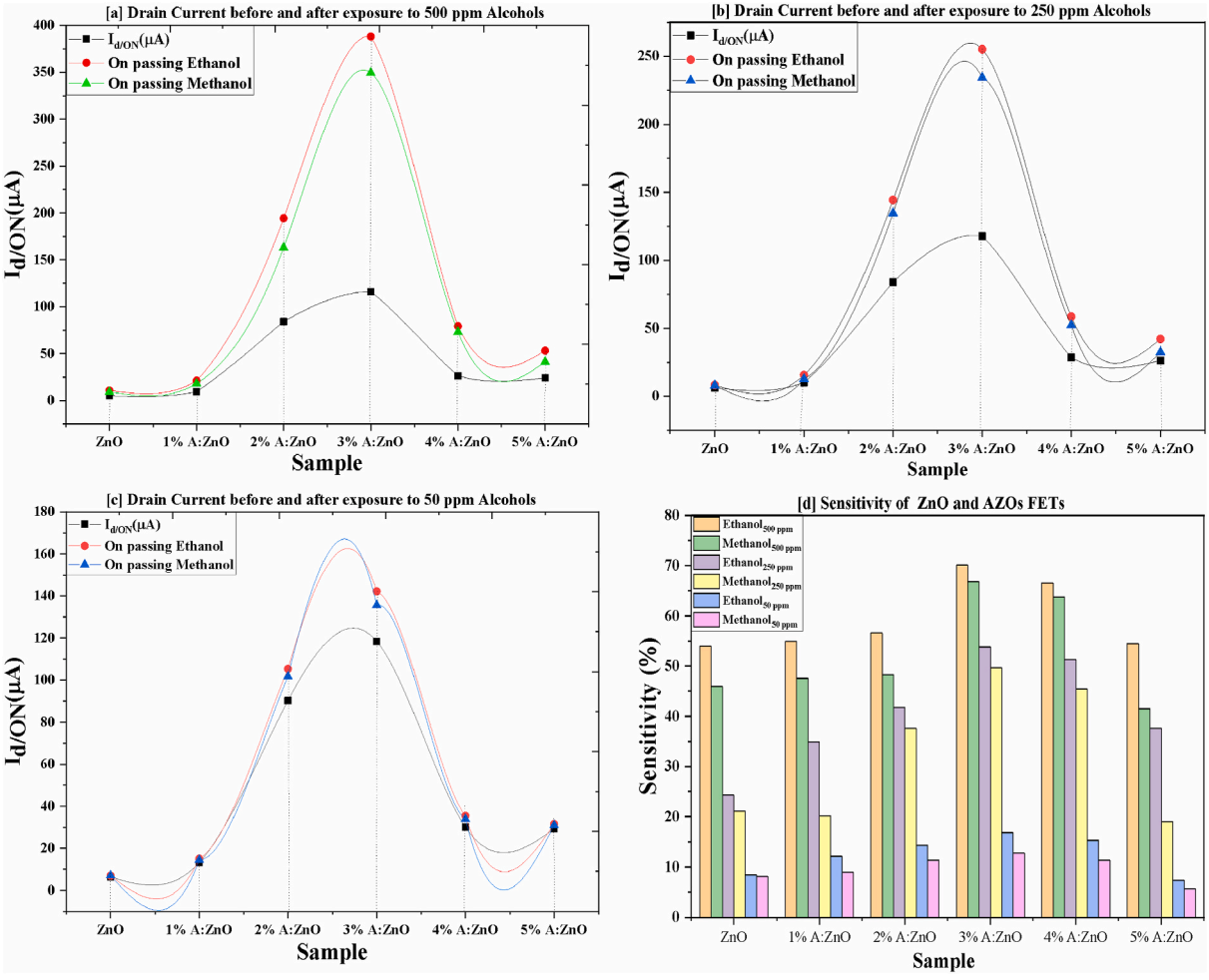

Fig. 14. [a-c] Drain current, [d] Sensitivity of ZnO and AZOs channeled FETs before and after exposure to various concentrations of alcohol.

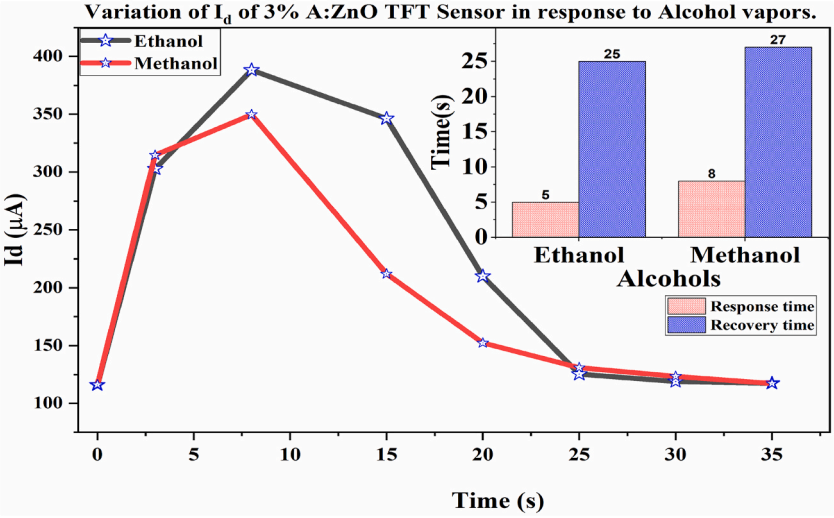

Fig. 15. Variation of Drain Current of 3 % A:ZnO channeled EDL dielectric polymer gated TFT in response to Ethanol and Methanol Vapors (500 ppm), and Bar chart showing Response and Recovery time of respective TFT embedded.

4. Conclusions

Pristine ZnO and 1–5% AZO nanostructured films are coated over transparent glass substrate using spin coating chemical method. The polycrystalline granny nature of ZnO and AZOs films is confirmed through the XRD pattern and the SEM images. These films exibit loosely packed porous and spherically arranged granny nanostructure with clearly visible grain boundary. The analysis of optical results obtained from the UV–vis spectrometer confirms the increase in the bandgap of the films, ranging from 3.12 to 3.16 eV. A small amount (optimal at 3 % by volume) of Al pioneered as dopant ionizes to Al^{3+} and replaces Zn^{2+} ions in the lattice thereby generating one free electron, resulting the increment of carrier concentration (with decreased resistivity). However, further increments in dopant concentration results in formation of neutral defect, reducing the number of electrically active Al and consequently increasing resistivity further.

Among the grown films, the most conductive was the 3 % Al-doped ZnO film, which was selected as the channel material for fabricating both two-terminal and three-terminal gas sensors. For the TFT application, a polymer electrolyte was utilized as the gate dielectric. This polymer electrolyte has the capability to induce ultra-high charge carriers on the surface of the Al:ZnO channel, thereby enhancing the performance of the TFT sensor.

The sensitivity of the two-terminal device to methanol vapor, when using the polymer electrolyte, showed a remarkable enhancement compared to ethanol vapor. This leads to conclude that the polymer electrolyte is hypersensitive to methanol vapor. Similarly, in the three-terminal gate-controlled field-effect device, the sensitivity and response/recovery times as well was improved.

Ultimately, the study concludes that a 3 % aluminum doping concentration is most effective for sensing ethanol and methanol. Additionally, TFT sensors are identified as promising candidates for gas sensing due to their ability to precisely control channel current with gate-source voltage bias, offering advantages such as faster response times and increased sensitivity to alcohol vapors.

Data Availability Statement

The data that support the findings of this research are openly available in [Fabrication-of-Alcohol-Sensor] at the link below: https://github.com/raaju1993/Fabrication-of-Alcohol-Sensor.
Feel free to analyze it according to the specific data sharing practices and requirements of your study.

CRediT authorship contribution statement

Raju Bhattarai: Writing – original draft, Visualization, Software, Resources, Methodology, Investigation, Funding acquisition, Formal analysis, Data curation, Conceptualization. **Ram Bahadur Thapa:** Visualization, Software, Resources, Methodology, Investigation, Funding acquisition, Formal analysis, Data curation. **Deependra Das Mulmi:** Supervision, Investigation. **Rishi Ram Ghimire:** Writing – review & editing, Validation, Supervision, Project administration, Methodology, Formal analysis, Conceptualization.

Declaration of competing interest

The authors declare that they have no known competing financial interests or personal relationships that could have appeared to influence the work reported in this paper.

Acknowledgments

We are grateful to "Nepal Academy of Science and Technology (NAST)" for providing us lab-access for our research work. We would also like to acknowledge Associate Professor Dr. Bhim Kafle and Assistant Professor Manoj Pandey, Kathmandu University, for electrical measurement using Keithley 2400 Source meter. We would also like to thank Dr. Tista Prasai Joshi, Senior Scientist, NAST and Rashmi Koju, "Research Center for Eco-Environment Sciences, Chinese Academy of Sciences, Beijing, China for providing space" and helping carrying out the SEM and EDX. We would like to extend our gratitude to Mr. Sujan Thapa from Torrens University, Adelaide and Arjun Shrestha from Flinders University, Adelaide for their assistance in reviewing our work. Additionally, we appreciate Mr. Dikshant Dhakal from Texas State University, San Marcos, Texas for providing technical support.

References

[1] X. Liu, S. Cheng, H. Liu, S. Hu, D. Zhang, H. Ning, Sensors 12 (7) (2012) 9635–9665.
[2] V.L. Patil, D.S. Dalavi, S.B. Dhavale, et al., Sensor Actuator Phys. 340 (2022) 113546.
[3] S.G. Leonardi, Chemosensors 5 (2) (2017) 17.
[4] G.S. Hikku, R.K. Sharma, R.V. Willium, P. Thiruramanathan, S. Nagaveena, J. Taibah Univ. Sci. 11 (4) (2017) 576–582.
[5] A. Ahmed Al-Ghamdi, O.A. Al-Hartomy, M. El-Okr, A.M. Nawar, S. El-Gazzar, F. El-Tantawy, F. Yakuphanoglu, Spectrochim. Acta Mol. Biomol. Spectrosc. 131 (2014) 512–517.
[6] R.R. Ghimire, A.K. Raychaudhuri, Appl. Phys. Lett. 110 (2017) 052105.
[7] R.R. Ghimire, S. Mondal, A.K. Raychaudhuri, J. Appl. Phys. 117 (2015) 105705.
[8] S. Zafar, M. Lu, A. Jagtiani, Sci. Rep. 7 (2017) 41430.
[9] N. Liu, R. Chen, Q. Wan, Sensors 19 (2019) 3425.
[10] S.C. Navale, V.R.S. Mulla, S.W. Gosavi, S.K. Kulkarni, Sensor. Actuator. B Chem. 126 (2) (2007) 382–386.
[11] A.V. Babalola, V. Oluwasusi, et al., Heliyon 10 (1) (2024) e23190.
[12] R. Bhattarai, R.R. Ghimire, D.D. Mulmi, R.B. Thapa, Heliyon 10 (2024) e29222.
[13] J. Xu, J. Han, Y. Zhang, Y. Sun, B. Xie, Sensor. Actuator. B Chem. 132 (2008) 334–339.
[14] D.D. Mulmi, B. Dahal, H.Y. Kim, M.L. Nakarmi, G. Panthi, Optik 154 (2018) 769–776.
[15] M.H. Aslan, A.Y. Oral, E. Mensur, A. Gul, E. Basaran, Solar Energy Mater. Solar Cells 82 (2004) 543–552.
[16] I.G. Dimitrov, A.O. Dikovska, P.A. Atanasov, T.R. Stoyanchov, T. Vasilev, J. Phys. Conf. 113 (2008) 012044.
[17] E. Muchuweni, T.S. Sathiaraj, H. Nyakotyo, Heliyon 3 (4) (2017) e00285.
[18] A. Chelly, S. Glass, J. Belhassen, A. Karsenty, Results Phys. 48 (2023) 106445.
[19] Z.Q. Xu, H. Deng, Y. Li, Q.H. Guo, Y.R. Li, Mater. Res. Bull. 41 (2) (2006) 354–358.
[20] X. Zi-qiang, D. Hong, L. Yan, C. Hang, Mater. Sci. Semicond. Process. 9 (2006) 132–135.
[21] Y.Z. Su, M.Z. Zhang, X.B. Liu, Z.Y. Li, Int. J. Electrochem. Sci. 7 (2012) 4158–4170.